JOURNAL OF GEOPHYSICAL RESEARCH, VOL. 102, NO. B12, PAGES 27,439-27,451, DECEMBER 10, 1997

Upper mantle structure of the southwest Pacific from regional waveform inversion

Yingbiao Xu and Douglas A. Wiens

Department of Earth and Planetary Sciences, Washington University, St. Louis, Missouri

Abstract. We determine the upper mantle seismological structure of the southwest Pacific by inverting complete regional seismograms recorded by the Southwest Pacific Seismic Experiment, a deployment of 12 broadband seismographs in the Fiji, Tonga, and Niue islands. We first present a method to invert entire seismic waveforms for a laterally homogeneous velocity structure. Partial derivatives are computed using an efficient reflectivity code for differential seismograms [*Randall*, 1994], and a conjugate gradient method is used to perform the nonlinear inversion. Band pass-filtered (10-55 mHz) vertical and radial component seismograms, extending from the *P* arrival to the surface waves, are used to constrain the structure. Waveforms are selected to provide regional distance (400-1500 km) propagation paths predominantly within one of the tectonic regions of the southwest Pacific. Source depths ranging from 10 to 240 km allow the deeper regions of the model to be resolved with relatively short path lengths. Results show extremely large lateral variability in the upper mantle structure of the southwest Pacific. The inactive South Fiji Basin shows upper mantle velocities much lower than those previously observed for the Pacific lithosphere of a similar age. The North Fiji and Lau Basins, containing active back arc spreading systems, show upper mantle shear velocities as slow as 3.8 km s^{-1}. The exceptionally low seismic velocities in the active back arc regions may represent the slowest upper mantle velocities in the world. The velocity difference between the active back arc basins and the old Pacific lithosphere immediately east of the Tonga Trench is maximum at 30-90 km depth, with a variation of ~18%, indicating partial melting in this depth range. Velocity heterogeneity of >4% extends to a depth of 170 km. Velocity structure below 220 km depth is poorly resolved, but there is some evidence of a 2% difference extending to depths of 350 km.

1. Introduction

Lateral and depth-dependent variations in the upper mantle velocity structure have important consequences for geochemical and geodynamic modeling of the Earth. The variation in seismic wave velocity should represent thermal and chemical heterogeneities in the mantle. Global and regional three-dimensional (3-D) tomography have provided large-scale maps of the lateral heterogeneity in the upper mantle [e.g., *Woodhouse and Dziewonski*, 1984; *Montagner and Tanimoto*, 1991; *Woodward and Masters*, 1991; *Zhang and Tanimoto*, 1992; *Su et al.*, 1994; *Trampert and Woodhouse*, 1995] . These global models are capable of resolving the Earth's structure down to scale lengths of ~1000-2000 km.

While global studies have successfully revealed the large-scale structure of the Earth, better resolution can be obtained for important regions using more closely spaced seismographs and regional waveform inversion methods [e.g., *Nolet et al.*, 1994]. Many global models underestimate the magnitude of lateral heterogeneity in the upper mantle when compared with models determined with 1-D methods, especially with regard to the regions that are characterized by extremely large amplitude lateral heterogeneity, like the southwest Pacific.

The characteristics and depth extent of the low-velocity zone under spreading centers still remains an outstanding concern [*Nolet et al.*, 1994]. There has been a long-standing controversy about how deep the signature of an oceanic spreading center extends, with some investigators favoring slow velocity anomalies limited to depths of <100 km [*Zhang and Tanimoto*, 1992, 1993], whereas others suggest the slow velocities extend to depths of at least 300 km [*Su et al.*, 1992]. This question has considerable implications for our understanding of the dynamics of oceanic spreading centers [e.g., *Forsyth*, 1992; *Tanimoto and Stevenson*, 1994].

The Southwest Pacific Seismic Experiment, a deployment of 12 broadband Program for Array Seismic Studies of the Continental Lithosphere (PASSCAL) seismographs in the Fiji-Tonga region, represents an important opportunity to study the seismic velocity structure beneath the active North Fiji and Lau back arc spreading centers. In order to determine the magnitude and depth dependence of seismic velocity heterogeneity in this region we modeled upper mantle seismological structure within tectonic units of the southwest Pacific by inverting complete regional seismograms. The use of relatively short path lengths allows the heterogeneity to be well localized spatially. The use of entire waveforms extending from the *P* arrival to the Rayleigh wave allows good resolution of structure throughout a wide depth range since the fundamental mode Rayleigh wave is largely sensitive to shallow structure and the body wave phases are sensitive to deeper structure. In addition, the waveform inversion overcomes previous problems with windowing individual phases since the *S*, *sS*, and Rayleigh waves arrive at nearly the same time at this distance range. The large number of seismic sources at a variety of depths also allows the use of intermediate depth earthquakes as sources, facilitating the determination of structure at depths of 150-400 km.

Paper number 97JB02564.
0148-0227/97/97JB-02564$09.00

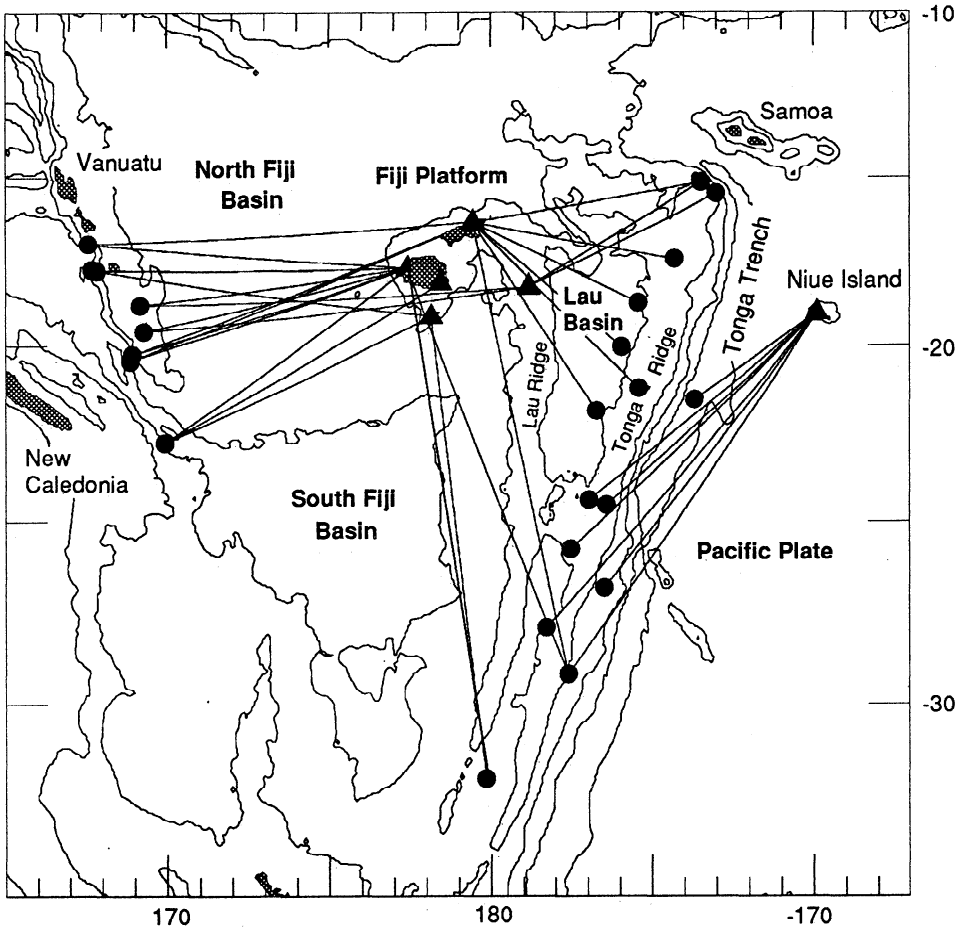

Figure 1. Simplified bathymetric map of the southwest Pacific with each of the major tectonic units delineated along with the 34 source-receiver paths used in this inversion. Solid dots represent the earthquake locations, and solid triangles mark the sites of broadband stations.

2. Waveform Inversion

2.1. Data

Data used in this study are from the Southwest Pacific Seismic Experiment [*Wiens et al.*, 1995] . Twelve broadband PASSCAL seismographs were deployed from November 1993 to December 1995 in the Fiji, Tonga, and Niue islands. Most stations consisted of a Streckeisen STS 2 seismograph deployed in a 1 m deep vault and a Reftek 24-bit data acquisition unit with Global Positioning System (GPS) timing. Data were recorded continuously at 25 Hz.

The active seismicity of the southwest Pacific provided numerous waveforms recorded at these stations suitable for waveform modeling. We selected a subset of these waveforms on the basis of the following criteria: (1) the source-receiver distance must be between 400 and 1500 km, such that there is little dependence on structure beneath 400 km depth; (2) the ray path must lie predominantly within one of the tectonic regions; and (3) the source must have a moderate seismic moment in order to avoid source complexity yet provide a reasonably accurate source location and focal mechanism. In this study a point source is assumed, and the temporal and spatial distribution of the moment release are not taken into account. Finally, (4) the waveforms must show a high signal-to-noise ratio. Waveforms were also selected to provide a reasonable number of quality waveform samplings of each region and to provide a range of source depths extending from 10 to 240 km. Figure 1 shows a simplified bathymetric map of the southwest Pacific with each of the major tectonic units delineated along with the source-receiver paths for each of the waveforms used in the inversion. The 68 waveforms selected were recorded at six different stations (Table 1) and resulted from 23 different earthquakes (Table 2).

In this study, only vertical and radial components are used to derive the velocity model. Our observations suggest that there is significant incompatibility between Rayleigh and Love wave dispersion results for this region and any isotropic model. In general, this is usually interpreted as evidence for anisotropy [*Anderson*, 1961; *Forsyth*, 1975; *Kirkwood and Crampin*, 1981]. At this stage the inversion result provides a first-order shear velocity structure. Since only vertical and radial components are included, this velocity should correspond closely to the SV velocity for an anisotropic inversion with transverse symmetry. We will extend this study to explicitly include the SH component by assuming transverse anisotropy in a later study.

2.2. Inversion Method

2.2.1. Waveform inversion methods. A variety of methods have previously been applied to determine the seismic velocity structure from waveforms. These include (1) a trial and error approach, which is usually applied when the structure can be

Table 1. Locations of Stations

Station	Code	Latitude, °N	Longitude, °E
Labasa, Fiji	LBSA	-16.3019	179.4506
Lautoka, Fiji	LTKA	-17.6878	177.4283
Lakeba, Fiji	LKBA	-18.2331	-178.8144
Kadavu, Fiji	KDVU	-19.0992	178.1629
Suva, Fiji	SUVA	-18.1147	178.4536
Niue Island	NIUE	-18.9794	-169.8764

described with relatively few unknowns or the forward calculations are demanding [e.g., *Zhao and Helmberger*, 1991], (2) iterative linearized inversion, which is applied by assuming that the true model is a small deviation from a starting model and by expanding the synthetic seismogram in a truncated Taylor series about the starting model [e.g., *Woodhouse and Dziewonski*, 1984] (our experience suggests that for the regional wavefom inversion the inverse problem may be highly nonlinear with the solution possibly being trapped in a local minimum if the starting model is not close to the actual Earth), and (3) Nonlinear inversion, which may be solved with a genetic algorithm or iterative gradient techniques. Using genetic algorithms in waveform inversion [e.g., *Sambridge and Drijkoningen*, 1992] has the advantage of being able to solve highly nonlinear problems, but it requires the forward calculation to be computationally efficient thereby excluding accurate synthetic methods for the regional waveform problem.

Other methods in nonlinear inversion use gradient information on the objective function, as in the steepest descent and the conjugate gradient methods, or curvature information on the objective function, as in the "Newton-type" methods. Gradient methods have been shown to be efficient for nonlinear waveform optimization [e.g., *Nolet et al.*, 1986; *Nolet*, 1990]. Compared with the linearized inversion method, the nonlinear gradient method is less restrictive for the starting model. However, it is a local optimization method, so it still requires a good a priori model which tends to reduce the nonlinear effects. Whether to use the Newton-type method [e.g., *Nishimura and Forsyth*, 1989; *Gaherty et al.*, 1996] or a gradient method [e.g., *Nolet et al.*, 1986] depends upon the size of inverse problem itself. The Newton-type method has a faster convergence rate because more information is used in searching for the minimum at the expense of more time being consumed in the evaluation of inverse of the quasi-Hessian matrix.

2.2.2. The conjugate gradient method. For large problems it is generally more efficient to use gradient methods [*Tarantola*, 1987]. In this study we adopt the conjugate gradient method to perform the nonlinear inversion. The conjugate gradient method has a linear convergence property, and the rate of convergence of the minimization depends on how many distinct groups of eigenvalues the Hessian matrix possesses. However, by using the partial conjugate gradient method the convergence rate is controlled by an improved condition number with the largest eigenvalue removed from consideration [*Luenberger*, 1972].

Since the theoretical background of the conjugate gradient method has been presented in numerous papers, we simply outline the main steps. Following *Tarantola* [1987], we define the objective function by

$$S(\mathbf{m}) = \frac{1}{2}\left\{\left[\mathbf{g}(\mathbf{m}) - \mathbf{d}_{\text{obs}}\right]^t \mathbf{C}_D^{-1}\left[\mathbf{g}(\mathbf{m}) - \mathbf{d}_{\text{obs}}\right] + (\mathbf{m} - \mathbf{m}_{\text{prior}})^t \mathbf{C}_m^{-1}(\mathbf{m} - \mathbf{m}_{\text{prior}})\right\} \quad (1)$$

where $\mathbf{g}(\mathbf{m})$ are synthetic seismograms, calculated using the reflectivity method [*Fuchs and Muller*, 1971; *Kennett*, 1983; *Randall*, 1994], $\mathbf{m}$ is the model parameter vector, $\mathbf{d}_{\text{obs}}$ are the observed data, $\mathbf{C}_D$ is the a priori data covariance matrix, $\mathbf{C}_m$ is thea priori model covariance matrix, and $\mathbf{m}_{\text{prior}}$ is the a priori estimate of the model parameters.

Table 2. Source Parameters of Earthquakes

Event	Date	Origin Time, UT	Latitude, °N	Longitude, °E	Depth,* km	Moment dyn cm
1	Aug. 11, 1994	1932:52.1	-21.840	-176.708	180.	8.4×10^{24}
2	July 28, 1995	1429:11.0	-21.182	-175.394	102.	4.3×10^{25}
3	Sept. 12, 1994	2243:50.7	-15.455	-172.990	20.	9.8×10^{24}
4	Feb. 24, 1994	1525:35.8	-17.421	-174.287	128.	1.8×10^{25}
5	Oct. 6, 1995	1139:34.8	-20.002	-175.921	209.	4.0×10^{25}
6	Aug. 25, 1995	1651:46.6	-18.686	-175.409	224.	11.6×10^{24}
7	Nov. 13, 1995	0738:42.6	-15.114	-173.473	10.	12.9×10^{24}
8	Feb. 11, 1994	2117:31.1	-18.773	169.169	206.	2.1×10^{26}
9	June 29, 1995	1224:3.2	-19.544	169.287	144.	9.3×10^{25}
10	Feb. 15, 1994	2111:56.4	-20.399	168.866	20.	5.9×10^{25}
11	Feb. 16, 1994	2203:8.9	-20.230	168.925	15.	1.2×10^{25}
12	July 24, 1994	1755:40.3	-16.966	167.574	21.	4.0×10^{25}
13	Oct. 1, 1994	1635:20.7	-17.745	167.682	17.	6.8×10^{25}
14	Oct. 1, 1994	1746:37.5	-17.768	167.830	10.	2.3×10^{25}
15	May 22, 1995	0345:4.7	-22.770	169.930	10.	1.5×10^{25}
16	Dec. 27, 1994	1732:50.8	-31.965	179.860	216.	4.0×10^{25}
17	Jan. 30, 1994	2057:43.4	-29.184	-177.589	44.	1.2×10^{25}
18	April 27, 1994	0923:26.2	-21.515	-173.667	41.	2.9×10^{25}
19	Jan. 14, 1995	0649:23.8	-27.929	-178.273	213.	4.2×10^{24}
20	Jan. 23, 1995	1016:18.5	-26.835	-176.472	10.	6.4×10^{24}
21	Oct. 14, 1995	0800:49.9	-25.758	-177.522	172.	2.2×10^{25}
22	Nov. 7, 1995	1355:35.8	-24.527	-176.400	15.	5.3×10^{24}
23	March 24, 1995	0711:40.3	-24.381	-176.945	115.	2.7×10^{24}

*Adjusted depth that was actually used for the waveform fitting in this paper.

The misfit is of least squares sense. The gradient $\partial S / \partial \mathbf{m}$ is

$$\mathbf{r} = \mathbf{G}^t \mathbf{C}_D^{-1}(\mathbf{g}(\mathbf{m}) - \mathbf{d}_{obs}) + \mathbf{C}_m^{-1}(\mathbf{m} - \mathbf{m}_{prior}) \quad (2)$$

and $\mathbf{G} = \partial \mathbf{g} / \partial \mathbf{m}$ is the matrix of differential seismograms which map the perturbation in model space to the perturbation in data space.

The Fletcher-Reeves method was used for implementing the conjugate gradient algorithm. The complete algorithm is given by *Luenberger* [1972]. In practice, inaccurate line searches, nonquadratic terms in the objective function, and rounding off errors may cause a poor eigenvalue structure and thus slow the convergence. To reduce the nonlinearity of the problem, we begin the inversion using the lowest-frequency band, and after the minimum of misfit is reached, we increase the frequency band [*Chapman and Orcutt*, 1985]. This procedure also has the advantage of providing a good fit across a wider range of frequencies and not simply fitting the dominant frequency.

2.2.3. Calculation of the partial derivatives. We use a reflectivity code that efficiently calculates the differential seismograms [*Randall*, 1994].

The differential seismogram

$$\frac{\partial g(t,m)}{\partial m} \quad (3)$$

represents the differential change in the seismogram for a differential change of a single model parameter or the sensitivity of the seismogram to a single parameter in the velocity model. When differential seismograms are computed, only a single layer at a time is perturbed and a difference approximation for the derivative is used, such as

$$\frac{\partial g(t,m)}{\partial m} \approx \frac{[g(t,m+\delta m) - g(t,m)]}{\delta m} \quad (4)$$

where δm represents the perturbed parameter in the velocity model. For an N-layered model, N+1 synthetic seismograms need to be calculated to construct differential seismograms, which is very time consuming for the brute force approach. *Randall* [1994] developed a technique to efficiently calculate the differential seismograms. The computation time of this technique is equivalent to computing three synthetic seismograms for a multilayered model, which reduces the work by $3/(N+1)$ or an ~90% savings for 30 layers as compared to the brute force approach.

The efficiency of this method is obtained by avoiding repeated computation of some terms in the transformed displacement. The model can be subdivided into regions above or below the perturbed layer. If the perturbed layer is above the source layer, the excitation term and the reflectivity of the region below the source layer will be unchanged. If the perturbed layer is below the source layer, the excitation term will again be unchanged, and the reflectivity of the region above the source and the receiver function term will be unchanged. If the perturbed layer is the source layer, all the terms will be perturbed. Three different methods are used to compose the final transformed displacement [*Randall*, 1989, 1994]. Two methods are distinguished by the recursion direction to compute the reflectivities R_D^{SN} and R_U^{fS} and the receiver function. The reflection matrices R_D^{SN} and R_U^{fS} represent the reflection of downward traveling waves from the layering below source depth and the reflection of upward traveling waves from the layering above source depth respectively. One recursion direction is thus called bottom up, and the other is top down. The third approach uses the intermediate results from the other two to reassemble R_D^{SN}, R_U^{fS}, and the receiver function.

2.2.4. Model parameterization. In order to compute the synthetic seismogram, we require both P and S velocity as well as density for each layer of the model. However, the seismograms are most sensitive to the shear velocity, as this largely controls the timing of the direct S phase and Rayleigh waves, which are generally the largest arrivals in the seismogram. The seismograms are less sensitive to the P velocity and density and including them as independent model parameters results in an underdetermined model. We therefore select the shear velocity in each layer as the model parameters to be solved. The P velocity structure is derived from the relationship $\alpha = \gamma\beta$, where γ is ratio of the P velocity to the S velocity. The γ is assumed to be depth-independent, and the best fitting γ is determined using a grid search between iterations. The ratios of the P velocities to the S velocities of all five tectonic regions are within the range of 1.80-1.83, which is close to the value derived from the preliminary reference Earth model (PREM) [*Dziewonski and Anderson*, 1981]. The density structure was also parameterized as a function of the shear velocity structure using the relationship $\rho = 0.32\gamma\beta + 0.77$ [*Berteussen*, 1977]. We do not attach any significance in the interpretation to the resulting density and P velocity structures, as they are merely auxiliary parameters included to allow computation of the forward model. We require that all waveforms traversing a given tectonic region be fit by the same structure. This introduces some slight misfit in the final synthetics, as small amounts of lateral heterogeneity within each region are ignored but ensures that the inverse problem is well constrained.

After a number of trials with various layer thicknesses we adopted a layer thickness of 20 km for the mantle. This value has the advantage of allowing better parameterization of strong gradient zones when compared to thicker layers, yet the inversion results indicate that the individual layers are still well resolved, particularly in the upper 200 km of the model. Since all regions considered in the model consist largely of oceanic lithosphere, we use a uniform crustal thickness of 10 km. A water layer is used in the model which is the average water depth for a particular tectonic region, as estimated from bathymetry maps (Lau Basin, 2.5 km; North Fiji Basin, 2.5 km; South Fiji Basin, 3.5 km; and Pacific Plate, 5.5 km).

3. A Priori Information

3.1. Tectonic Regions of the Southwest Pacific

As with most inverse procedures, it is necessary to incorporate some a priori knowledge in the inversion. This knowledge is used to supply necessary parameters, such as the Q model and source location, that are not well constrained by the waveforms themselves but may be constrained by other types of information. A priori velocity models are also used both as a starting model for the first iteration and to stabilize underdetermined parts of the inversion. The a priori models are developed from the known tectonic history of the regions, as discussed below.

3.1.1. North Fiji Basin. The North Fiji Basin is located between the New Hebrides trench, which marks the subduction of the India-Australia Plate under North Fiji Basin, and Fiji Platform. Active back arc spreading commenced 7.8 myr ago [*Malahoff et al.*, 1982], and two active spreading ridges (the central spreading ridge and the west Fiji ridge) have been identified. Along the central spreading ridge the average spreading rate varies from 50 mm yr^{-1} on the northern segment to 80 mm yr^{-1} on the central and southernmost segments. For the

west Fiji ridge, magnetic anomaly analysis indicates spreading rates of 40-50 mm yr^{-1} [*Auzende et al.*, 1990, 1994, 1995].

3.1.2. Lau Basin The Lau Basin is an active back arc basin bounded by the Lau Ridge on the west and the Tonga Ridge in the east. Several different spreading centers exist within the Lau Basin. These include the Vela Fa and Eastern Lau Spreading Centers (ELSC) in the south, the Central Lau Spreading Center which is propagating southward into crust formed by the ELSC, and the Northwest Lau Spreading Center. Magnetic anomalies in the central and southern regions suggest that spreading commenced ~4-6 Ma and that current spreading rates range from 65 to 90 mm yr^{-1} [*Taylor et al.*, 1996; *Parson and Wright*, 1996]. However, GPS data indicate that the Lau Basin is opening at a rate ranging from 90 to 160 mm yr^{-1}, suggesting it is the fastest spreading back arc basin known [*Bevis et al.*, 1995]. The discrepancy between the GPS rates and the magnetic anomaly rates may indicate either that considerable extension occurs off the ridge axes or that spreading rates have increased during the past few hundred thousand years [*Taylor et al.*, 1996].

3.1.3. South Fiji Basin The South Fiji Basin is now an inactive marginal basin which lies north of New Zealand and is bounded by the Lau-Colville Ridge to the east, the Fiji platform to the north and the Loyalty Rise and Three Kings Rise to the west. Seafloor spreading occurred in the northern part of the basin from 26 to 33 Ma, as determined from magnetic anomaly studies [*Weissel and Watts*, 1975].

3.1.4. Pacific Plate The Tonga-Kermadec Trench marks the subduction of the Pacific Plate under the Tonga Island Arc. To the east of trench is the old Pacific lithosphere. Magnetic anomalies have not been identified in this region, but it is thought to have been formed during the Cretaceous Quiet Zone ~110 Ma (P. Lonsdale, personal communication, 1995).

3.2. A Priori Velocity Models

For each tectonic region of the southwest Pacific we assign the a priori model from *Nishimura and Forsyth* [1989] according to the age of the lithosphere (the 0-4 Ma model is used for the Lau Basin and the North Fiji Basin; the 20-52 Ma model is used for the South Fiji Basin; and the 110+ Ma model is used for the Pacific Plate). The data used to construct these models were fundamental mode Rayleigh (20-125 s period) and Love wave (33-125 s) phase velocities from paths which traversed the Pacific. Pure path phase velocities for the seafloor of five age ranges (0-4, 4-20, 20-52, 52-110, and 110+ Ma) were derived from this data set, and each pair of Rayleigh and Love pure path phase velocities was fit to derive the models of shear wave velocity as a function of depth assuming transverse anisotropy.

We convert the structures given by *Nishimura and Forsyth* [1989] to isotropic velocity structures by averaging the horizontal and vertical velocities. These a priori isotropic structures are shown in Figure 2 and are also given in Table 3 along with their associated uncertainties. The models show large variations in upper mantle velocity, but the heterogeneity is reduced to <3% below 150 km, and the structures are completely identical below 190 km. However, the resolution of the *Nishimura and Forsyth* [1989] study is poor at the larger depths and is virtually unresolved below 150 km depth.

The a priori parameter covariance matrix is similar to that used by *Nishimura and Forsyth* [1989]

$$C_{mm}(r_i, r_j) = \sigma_i \sigma_j \exp\left[-\frac{(r_i - r_j)^2}{2\Delta^2}\right] \quad (5)$$

where σ_i is the standard deviation of the ith parameter, r_i is depth of the ith parameter, and Δ is correlation length.

The correlation assumed for parameters at two different depths depends only on the correlation length Δ, which we take to be 20 km. The standard deviations of the model parameters were derived from values listed on Table 4 [*Nishimura & Forsyth*, 1989]. Selection of the a priori data covariance matrix is quite arbitrary. The seismograms all have large signal-to-noise ratios, so the data errors are almost entirely due to mislocation and the approximation of the theory. Obviously, errors in the data of one seismogram are correlated because of common mislocation; however, estimating the form of the correlation is difficult. Therefore we assume that the data covariance matrix is diagonal. The standard deviations are all assigned to be 0.1, where the largest amplitude of the data is normalized to be 1. This approach automatically places much less weight on fitting the *P* waves than on fitting the *S* waves and surface waves, which have the largest amplitude. However, our main objective is to solve for the shear velocity, and the final inversion results show that the *P* waves are fit reasonably well anyhow.

3.3. *Q* Model

The age of the seafloor of the southwest Pacific ranges from very young (the Lau Basin and the North Fiji Basin) to very old (the Pacific lithosphere immediately east of the Tonga Trench). Different *Q* models were selected for tectonic regions with different ages of seafloor. The attenuation structures beneath the active back arc spreading center and South Fiji Basin are adopted from *Flanagan and Wiens* [1990, 1994] and *Flanagan* [1994]. These studies measured differential attenuation in the 0.01-0.08 Hz band between *sS* - *S* and *sScS* - *ScS* phase pairs to characterize the variation of attenuation with depth beneath the Lau back arc spreading center and beneath five other inactive back arc basins. From these results we adopt a Lau Basin and

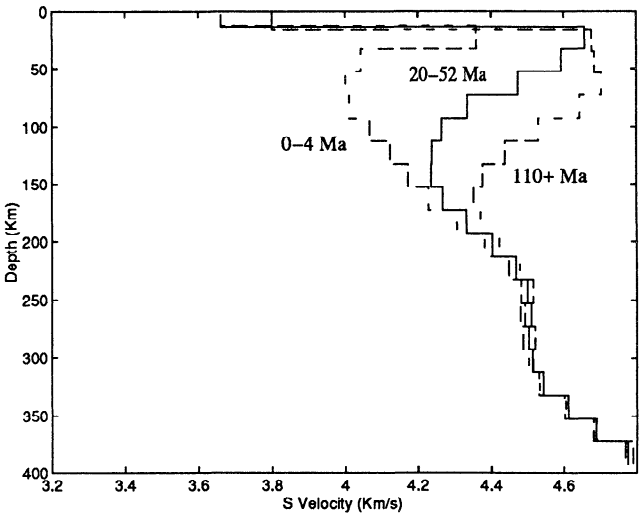

Figure 2. Diagram showing the isotropic velocity models for different ages of seafloor, which were adopted as a priori models in this study. Upper mantle structures are derived from a pure path study of Rayleigh and Love wave propagation in the Pacific [*Nishimura and Forsyth*, 1989] by averaging the horizontal and vertical velocities from a transverse anisotropy model. A uniform crust with thickness of 10 km is added on the top of the upper mantle structure. A water layer is used in the model with the average water depth for a particular tectonic region, as estimated from bathymetric maps.

Table 3. A Priori Isotropic Structures and Their Associated Uncertainties

	Region 0-4 Ma, km s^{-1}		Region 20-52 Ma, km s^{-1}		Region 110+ Ma, km s^{-1}	
Depth, km	β	σ	β	σ	β	σ
0-10	3.663	0.100	3.662	0.100	3.800	0.050
10-30	4.358	0.082	4.657	0.050	4.676	0.050
30-50	4.043	0.074	4.591	0.050	4.684	0.050
50-70	4.000	0.083	4.473	0.050	4.703	0.050
70-90	4.011	0.087	4.333	0.050	4.642	0.050
90-110	4.067	0.091	4.264	0.050	4.529	0.050
110-130	4.124	0.094	4.238	0.050	4.437	0.050
130-150	4.172	0.096	4.237	0.050	4.376	0.050
150-170	4.229	0.098	4.268	0.060	4.352	0.060
170-190	4.306	0.099	4.332	0.060	4.370	0.060
190-210	4.381	0.100	4.402	0.060	4.422	0.060
210-230	4.448	0.100	4.467	0.060	4.478	0.060
230-250	4.481	0.100	4.498	0.060	4.515	0.060
250-270	4.493	0.100	4.510	0.060	4.481	0.060
270-290	4.486	0.100	4.502	0.060	4.520	0.060
290-310	4.502	0.100	4.514	0.060	4.515	0.060
310-330	4.531	0.100	4.543	0.060	4.532	0.060
330-350	4.600	0.100	4.611	0.060	4.605	0.060
350-370	4.679	0.100	4.687	0.060	4.689	0.060
370-390	4.768	0.100	4.774	0.060	4.788	0.060

North Fiji Basin Q model which assumes Q = 25 from 0 to 150 km depth, and Q = 152 from 151 to 400 km. For the South Fiji Basin we use the Q model of Q = 46 down to 150 km and Q = 152 from 151 to 400 km. For the older Pacific Plate we use a Q model with Q = 80 between the surface and 220 km and Q = 144 between 220 and 400 km. This model for the Pacific Plate is generally similar to PREM [*Dziewonski and Anderson,* 1981]. Since the data in this study are low-pass filtered at 0.055 Hz, and the observed and synthetic data are normalized in the inversion, the effect of the Q model on the results is minimal.

3.4. Source Location and Focal Mechanism

In this study the earthquake location is taken from the preliminary determination of epicenters (PDE) monthly bulletin, and the depth and the focal mechanism are taken from the Harvard centroid moment tensor (CMT) catalog [*Dziewonski et al.*, 1981] . For shallow earthquakes the depth is adjusted slightly during the first stages by comparison with synthetic seismograms. We only use earthquakes for which both the vertical and the radial component amplitudes are well fit in order to minimize the error caused by focal mechanism uncertainties.

Table 4. Upper Mantle Shear Velocity Structures and Their Associated Errors of Southwest Pacific from Regional Waveform Inversion

	Lau Basin, km s^{-1}		North Fiji Basin, km s^{-1}		South Fiji Basin, km s^{-1}		Pacific Plate, km s^{-1}	
Depth, km	β	σ	β	σ	β	σ	β	σ
0-10	3.370	0.017	3.451	0.010	3.361	0.018	3.772	0.018
10-30	3.991	0.013	4.183	0.006	4.232	0.014	4.545	0.013
30-50	3.786	0.011	4.063	0.009	4.244	0.010	4.612	0.012
50-70	3.834	0.018	3.989	0.017	4.278	0.017	4.644	0.018
70-90	3.841	0.021	3.940	0.020	4.263	0.019	4.568	0.022
90-110	3.882	0.023	3.945	0.022	4.190	0.022	4.467	0.025
110-130	3.946	0.023	3.989	0.022	4.203	0.023	4.400	0.025
130-150	4.024	0.031	4.038	0.021	4.240	0.022	4.354	0.026
150-170	4.144	0.028	4.151	0.021	4.282	0.029	4.338	0.030
170-190	4.271	0.037	4.281	0.028	4.301	0.033	4.350	0.029
190-210	4.341	0.034	4.383	0.025	4.373	0.032	4.396	0.031
210-230	4.391	0.041	4.418	0.032	4.487	0.030	4.465	0.031
230-250	4.445	0.046	4.472	0.034	4.528	0.035	4.508	0.036
250-270	4.464	0.048	4.513	0.036	4.560	0.034	4.478	0.036
270-290	4.470	0.052	4.528	0.036	4.579	0.035	4.544	0.034
290-310	4.499	0.056	4.571	0.037	4.594	0.035	4.579	0.035
310-330	4.530	0.061	4.586	0.038	4.618	0.036	4.631	0.036
330-350	4.589	0.065	4.633	0.040	4.647	0.037	4.685	0.036
350-370	4.651	0.072	4.668	0.044	4.663	0.035	4.719	0.036
370-390	4.694	0.076	4.751	0.047	4.722	0.029	4.747	0.041

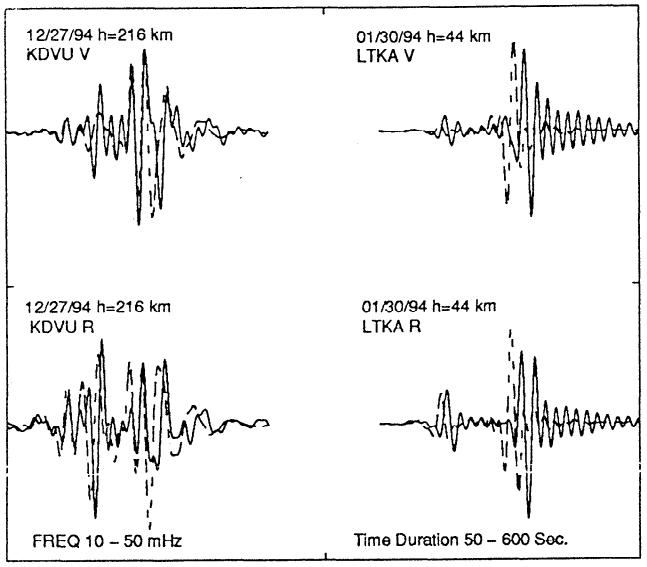

Figure 3. Comparisons of waveform fit between the observed data (solid line) and the synthetic data (dashed line) calculated using the a priori velocity model (20-52 Ma) for two paths crossing the South Fiji Basin. Vertical and radial components are shown for each earthquake. (left) One earthquake was located at intermediate depth (216 km), and (right) the other was located at a shallow depth (44 km). Each waveform extends from 50 to 600 s following the origin time of the event. Note the poor fit of the body waves and the Rayleigh wave, indicating that the actual structure is significantly slower than the a priori model.

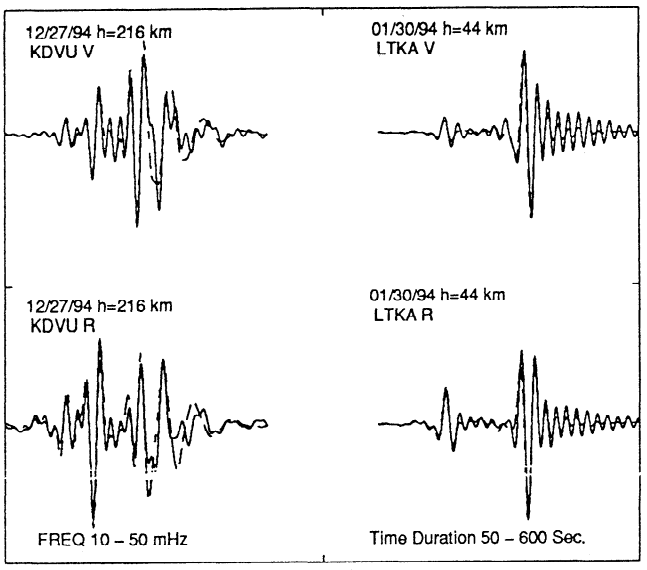

Figure 4. Same as Figure 3, with synthetic data calculated using the final South Fiji Basin model from the nonlinear inversion, as shown in Figure 5 and Table 4.

For the regional waveform inversion the largest uncertainty in the velocity structure may come from possible source mislocation. To reduce the possibility of large mislocation, only moderate earthquakes ($5.5 < M_W < 6.8$) are included in the inversion. Earthquakes with a large difference between the PDE monthly and weekly bulletin locations are excluded. Fortunately, we found that given these criteria, the waveforms from a large number of epicenters and paths can be fit reasonably well, indicating that the relative mislocation between earthquakes is small.

We also had the opportunity to check for systematic mislocation of earthquakes in the Tonga Trench when a well-located PDE earthquake (date: October 31, 1994; origin time: 2304:7.69UT; M_W: 5.4) occurred near a deployment of ocean bottom seismographs (OBS) in the region. Four OBSs were located within 100 km of the epicenter and spanned a wide range of azimuths. We added these four arrivals to the PDE data set and obtained a location which was shifted westward by 10 km with respect to the PDE monthly location. On the basis of this information, as well as on the basis of the consistency of the synthetics with the data for a wide variety of source receiver paths, we suggest that the uncertainty in the monthly epicentral locations for earthquakes of the size used in this study is of the order of 10 km. The effect of the epicentral uncertainty on the derived seismic structure depends on the path length. For the Lau Basin structure, determined mostly on the basis of path lengths of ~600 km, a 10 km uncertainty suggests a 1.5% uncertainty in the velocity structure. For other regions the path lengths are frequently >1000 km, suggesting that the location uncertainty contributes a <1% uncertainty to the velocity structure.

3.5. Inversion Result

As an example of our procedure, Figures 3 and 4 show waveform fits from the South Fiji Basin inversion for a shallow and an intermediate depth earthquake. Figure 3 shows the observed (solid lines) and synthetic data calculated with the a priori model (the 20-52 Ma velocity structure shown in Figure 2). Figure 4 shows the fit of the inversion result. The shallow earthquake (January 30, 1994) waveforms are dominated by the direct *P* phase and the fundamental mode Rayleigh wave. The *S* phase arrives at the beginning of the Rayleigh wave train. For the December 27, 1994, intermediate earthquake, phase separation is more clear, and the *P*, *sP*, *S*, and fundamental Rayleigh waves are somewhat separated. Comparison between Figures 3 and 4 shows that the a priori structure is much too fast, particularly at shallow depths which most influence the fundamental Rayleigh wave. The final structure, which is much slower than the a priori structure above 150 km depth, provides a good fit (Figure 4).

The computed oceanic upper mantle shear velocity structures in the four regions are shown in Figure 5. They are also given in Table 4 along with their associated errors obtained from the a posteriori parameter covariance matrix. A parameter is nonresolvable when the a posteriori variance is equal to the a priori variance [*Tarantola*, 1987]. In this sense all four models are resolved down to 400 km. The resolution decreases with depth as expected. The upper 200 km of the structure are well resolved by this data set. Figure 6 also gives some insight into how the uncertainties at various depths are correlated. For example, the crustal velocity of the back arc basins is low compared with normal oceanic crust. However, the correlation matrices show that the velocity of the crust and the velocity of the uppermost mantle just below the crust are negatively correlated. This means that the two velocities are not independently resolved, but rather, only a linear combination of those two velocities are resolved in the frequency range used in this study. An increase in the crust velocity in the final model will further reduce the velocity of the uppermost mantle just beneath the crustal layer.

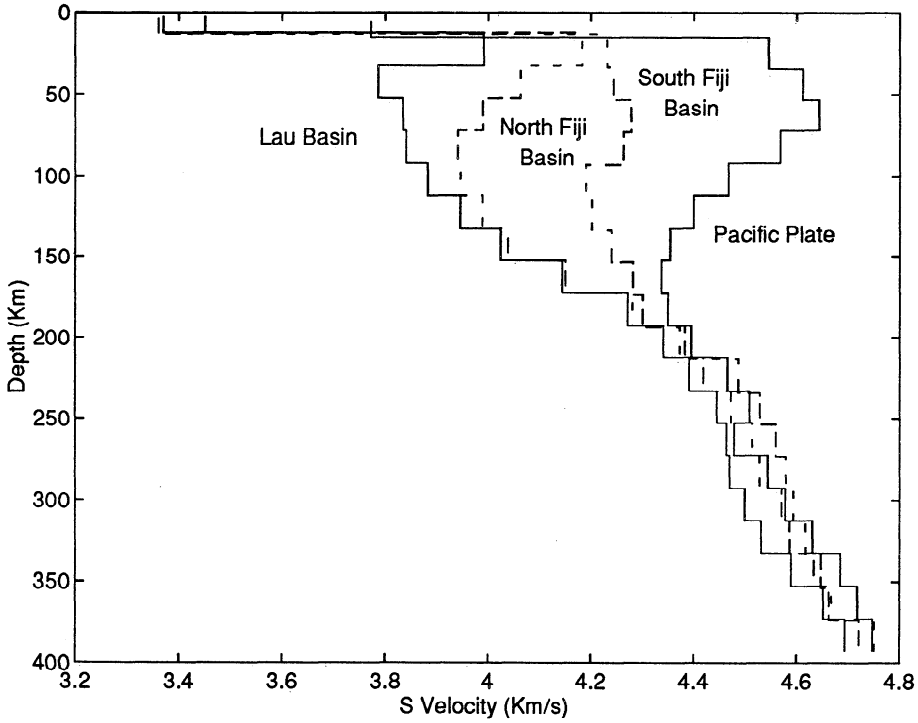

Figure 5. Regional waveform inversion result showing the shear wave velocity models of the Lau Basin, the North Fiji Basin, the South Fiji Basin, and the Pacific Plate regions as a function of depth. Back arcs with active spreading centers (the Lau Basin and the North Fiji Basin) show exceptionally slow seismic velocities in the upper mantle. Extremely large heterogeneity is indicated between the Lau Basin and the old Pacific Plate in the uppermost mantle.

4. Discussion

4.1 The Structure of Older Lithosphere: Pacific Plate and South Fiji Basin

The velocity structure of the Pacific Plate east of Tonga determined in this study is very similar to that determined for the old oceanic lithosphere by previous studies. Indeed, it does not deviate much from the a priori model taken from *Nishimura and Forsyth* [1989] despite the low variance of the result. The shear wave velocity ranges from 4.55 to 4.64 km s^{-1} from the Moho to 70 km depth. This is similar to the *Sn* velocity of 4.65 km s^{-1} found by the Negendi seismic refraction experiment in nearly the same region [*Shearer and Orcutt*, 1986] and similar to the lid velocity of 4.54 km s^{-1} found for the entire western Pacific in model PA2 [*Lerner-Lam and Jordan*, 1987]. These results can also be compared to anisotropic models of the old Pacific lithosphere, which have found lid SV velocities (bu) of 4.54 to 4.63 km s^{-1} [*Nishimura and Forsyth*, 1989] and 4.65 km s^{-1} [*Gaherty et al.*, 1996](Figure 7).

Because earthquakes with a wide range of depths were used to constrain the structure in this study, including some earthquakes within the low-velocity zone, tight constraints on the structure from 100 to 200 km depth are obtained [*Van Heijst et al.*, 1994]. The lower boundary of the lid appears to be smooth and not discontinuous, such that the precise thickness of the lithospheric plate cannot be reliably determined. If we choose the depth of the largest negative velocity gradient to represent the lower bound of the lithospheric plate, we obtain a plate thickness of 90 km, consistent with expectations based on thermal models [*Sclater et al.*, 1981; *Stein and Stein*, 1994]. The minimum velocity in the low-velocity zone occurs at 160 km depth and is slightly higher than that found in previous models, and no distinct base of low-velocity zone is found. The velocity structure of the Pacific Plate below 200 km is in good agreement with PA2 and PA5.

In contrast to the Pacific lithosphere model, the South Fiji Basin model deviates considerably from the a priori model derived from similarly aged lithosphere in the Pacific Ocean. The a priori model shows a lid with similar velocities to the old Pacific lithosphere, whereas the South Fiji Basin model shows a lid with velocity ~9% slower than the old Pacific lithosphere. The velocity remains considerably lower than the a priori model down to a depth of 130 km and remains lower than the Pacific lithosphere down to a depth of 200 km. Below 200 km, there is no resolvable difference between the South Fiji Basin and the old Pacific upper mantle. A previous surface wave study also found relatively slow upper mantle seismic velocities for the South Fiji Basin [*Sundaralingam*, 1986], and the South Fiji Basin generally shows slow upper mantle velocities on global phase velocity maps [e.g., *Trampert and Woodhouse*, 1995].

These results suggest that the uppermost mantle structure of back arc basins is slower than oceanic lithosphere of an equivalent age. Some degree of the discrepancy between the a priori model and the final model results because the a priori model averages the SH and SV structures of *Nishimura and Forsyth* [1989], whereas our *S* velocity structure is close to an SV structure when transverse isotropy is assumed. However, our final model is still considerably slower than their SV structure for the young Pacific lithosphere. The slow upper mantle velocities of inactive back arcs may result from geochemical differences between back arc mantle and normal oceanic lithosphere in that back arcs are created in the vicinity of subducting slabs and thus may be exposed to fluxing by slab volatiles. When compared to

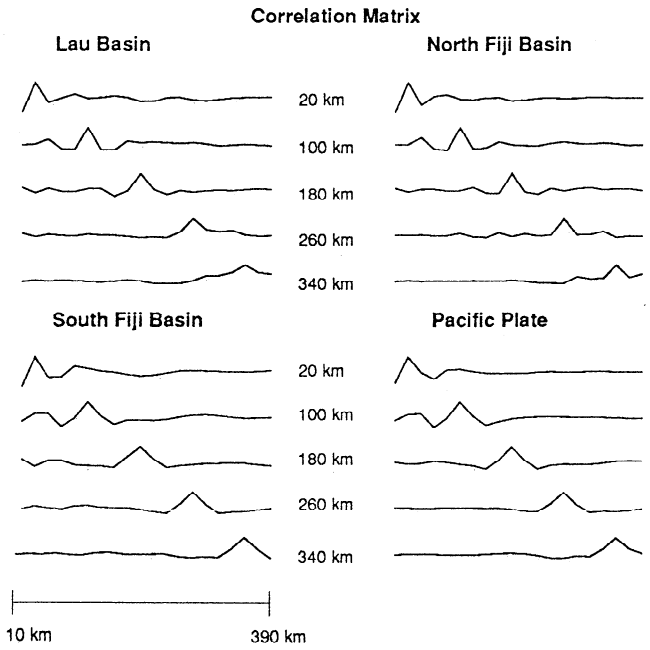

Figure 6. Resolution kernels for each of the models derived in the inversion. Each region shows the kernel (row of the correlation matrix) for 20, 100, 180, 260, and 340 km depth. Each depth is the depth of the middle of one layer. For each trace the horizontal scale ranges from 10 to 390 km. Kernels are from the posteriori correlation matrix, and by definition, the largest amplitude of each trace is normalized to 1.

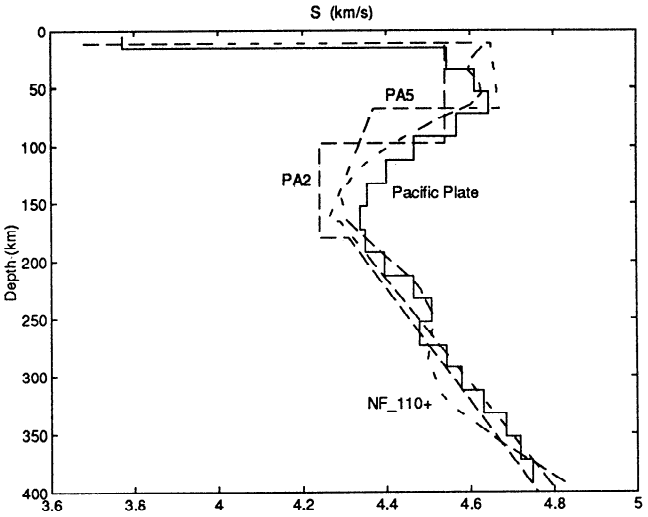

Figure 7. Comparison of the velocity structure for the old Pacific upper mantle derived in this study to other oceanic upper mantle velocity models. PA2[*Lerner-Lam and Jordan*, 1987] is a western Pacific model designed to fit Rayleigh waves. PA5[*Gaherty and Jordan*, 1996] is an SV velocity structure from a transverse anisotropic model for the Tonga-Hawaii path. NF_110+ [*Nishimura and Forsyth*, 1989] is a vertical *S* velocity structure for the 110+ Ma portion from a regionalized transverse anisotropic model of the Pacific. The Pacific model derived in this study is in generally good agreement with previous models.

normal mid-ocean ridge basalts, back arc basin basalts show subtile but distinctive differences, including large ion lithophile enrichment and the presence of excess volatiles. These effects are generally attributed to the slab [*Hawkins and Melchior*, 1985; *Sinton and Fryer*, 1987; *Hawkins*, 1995]. Volatiles generally have the effect of lowering the melting temperature and the seismic velocity [*Wyllie*, 1979; *Thompson*, 1992; *Nolet*, 1995]. The generally low upper mantle velocities of the inactive South Fiji Basin may indicate that marginal basins retain significant upper mantle volatiles for millions of year after back arc spreading ceases and at considerable distances from present-day subduction zones.

4.2. Shallow Structure Beneath Active Back Arc Spreading Centers

The upper mantle shear velocity is extremely low beneath the Lau Basin and the North Fiji Basin, which contain active spreading centers. The slowest velocities are found at depths between 30 and 90 km and reach as low as 3.8 km s^{-1} beneath Lau Basin and 3.95 km s^{-1} beneath the North Fiji Basin. These velocities are lower than the a priori model, derived from Pacific lithosphere of a similar age, and may represent the slowest upper mantle anywhere in the world. However, these results are compatible with previous work in the area, including *P* wave travel time studies that show *P* velocities as low as 7.3 km s^{-1} beneath the North Fiji Basin [*Dubois et al.*, 1973] and 7.1 km s^{-1} beneath the Lau Basin [*Aggarwal et al.*, 1972]. A surface wave study by *Sundaralingam* [1986] also showed an *S* velocity of 4.0 km s^{-1} for both the North Fiji Basin and the Lau Basin from the uppermost mantle to 220 km depth. Considering the averaging over a large depth range and the fact that most of his paths sampled several tectonic regions, this result is consistent with our study.

The Lau Basin upper mantle structure is considerably slower than the a priori model derived from the Pacific Ocean

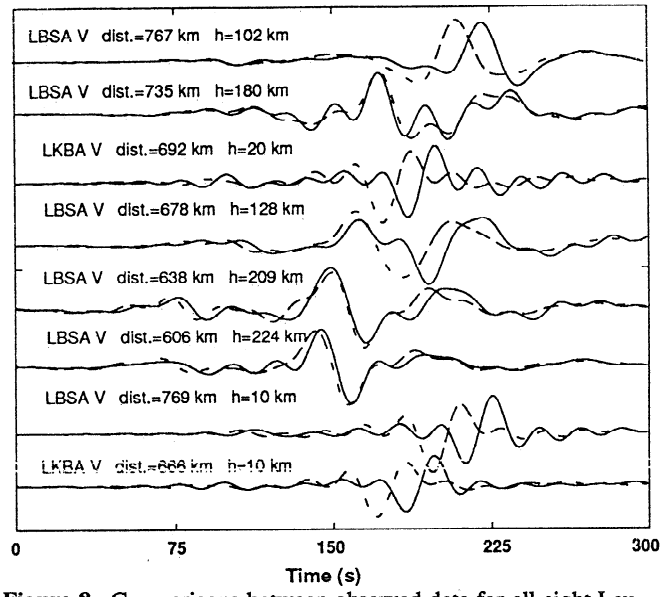

Figure 8. Comparisons between observed data for all eight Lau Basin paths (solid lines) and synthetic data (dashed lines) calculated with the a priori model for 0-4 Ma seafloor. Although radial data were also inverted, only vertical waveforms are shown here. Labels above each waveform give the station code, component, epicenter range, and hypocenter depth, respectively. Substantial misfit is found for the fundamental mode Rayleigh wave, indicating that the actual velocities are slower than the a priori model.

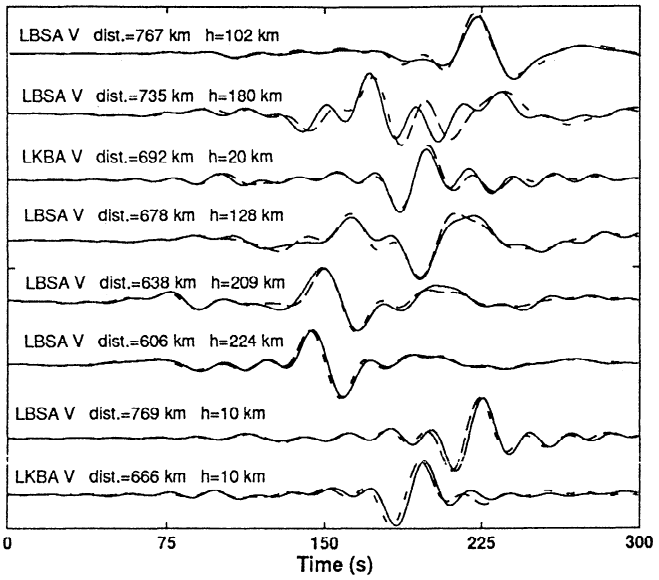

Figure 9. Same as Figure 8, except that synthetics are calculated with the final Lau Basin model determined in the inversion, as shown in Figure 5 and Table 4.

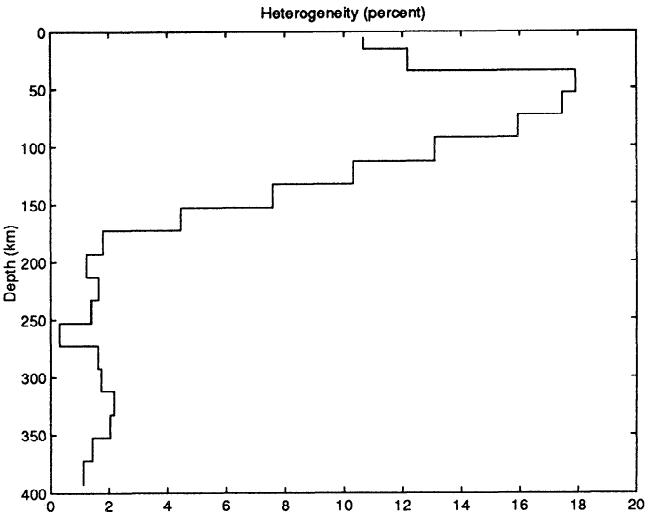

Figure 10. Heterogeneity between the active Lau Basin and the old Pacific upper mantle as a function of depth. The heterogeneity reaches its maximum of ~18% at a depth range of 30-70 km, and heterogeneity >4% is confined to depths shallower than 170 km. A small level of heterogeneity (2%) persists to depths of 350 km. The large degree of heterogeneity found for depths of 30-90 km results from partial melting associated with seafloor spreading in the Lau back arc.

lithosphere of a similar age. The difference between the a priori model and the result of this inversion is very clear in the data. As a comparison, waveform fits for all the Lau Basin paths are shown in Figures 8 and 9. Figure 8 shows the fit with the a priori model, taken from the 0-4 Ma Pacific lithosphere. The waveforms are dominated by the *S* arrival and the fundamental model Rayleigh wave; the fit to the *S* wave from the deeper earthquakes is fairly good, but the Rayleigh wave is poorly fit, indicating that the Lau Basin structure is significantly slower than the 0-4 Ma Pacific model. Figure 9 shows the much better fit that is obtained from the model derived in the inversion, which is significantly slower in the upper 150 km.

The slower seismic velocities found in this study relative to the *Nishimura and Forsyth* [1989] study may reflect a difference in methodology or may suggest that actively spreading back arc basins show slower upper mantle velocities than mid-ocean ridges. In our study the ray paths were selected to be predominantly within one of the tectonic zones. This may give a higher resolution for the velocities in regions of extreme velocity anomalies when compared to models derived from pure path assumptions based on large-scale regionalization. Another difference between the studies is the neglect of anisotropy in this study. We suggest that anisotropy does not play a large role in the difference between the two studies since under the transverse anisotropy assumption the anisotropy parameter x increases with the age of the seafloor [*Nishimura and Forsyth*, 1989]. The amplitude of ξ is quite small for the region with the age of seafloor range 0-4 Ma in the *Nishimura and Forsyth* [1989] model.

Extremely large heterogeneity exists at these depths between the Lau Basin and the Pacific Plate immediately east of the Tonga Trench. The difference between the Lau Basin and the Pacific Plate reaches a maximum at ~18% at depths of 30-70 km (Figure 10). The back arc basins remain slower than both the a priori model and the Pacific lithosphere down to a depth of ~200 km, but the heterogeneity is reduced to ~2% at the bottom of this range. This result is also consistent with recent *P* wave tomography results beneath the Lau Basin [*Zhao et al.*, 1997] using the Southwest Pacific Seismic Experiment stations as well as arrival times from a 3 month deployment of 25 ocean bottom seismographs.

The extremely slow velocities found in the back arc regions are undoubtably due to the formation of partial melt beneath the back arc spreading centers. The depths of the slowest anomalies and largest velocity differences with respect to the Pacific lithosphere is 30-90 km. These are the same depths which are thought to represent the primary magma genesis region for basaltic magmas at an oceanic spreading center [*McKenzie and Bickle*, 1988; *Tanimoto and Stevenson*, 1994; *Shen and Forsyth*, 1995]. We find that the lid above the low-velocity magma-producing region must be very thin, of the order of 10-20 km.

4.3 Depth Extent of the Slow Velocity Anomaly Beneath Back Arc Basins

Both the Lau and North Fiji Basins show velocities that are much lower than the old Pacific plate down to a depth of 170 km (Figure 5). The back arc basin structures are also much lower than the a priori model based on the 0-4 Ma Pacific lithosphere throughout this depth range. The use of intermediate depth earthquakes and body wave phases probably provides better resolution at depths >100 km than the *Nishimura and Forsyth* [1989] method, which was based on fundamental mode surface waves. Figure 11 illustrates a test of the resolution of our model to structure in the 100-170 km depth range. We constructed a new structural model (model nfb-pac, which is shown in Figure 11a) to test whether the differences between the back arc basins and the old Pacific lithosphere could be confined to depths shallower than 150 km. This model is identical to the North Fiji Basin (nfb) structure above 90 km, to intermediate structures between the nfb and the Pacific structure between 90 and 150 km depth, and to the Pacific structure below 150 km. Figure 11b shows a comparison of the fit to the data from an intermediate depth earthquake with a path traversing the North Fiji Basin for

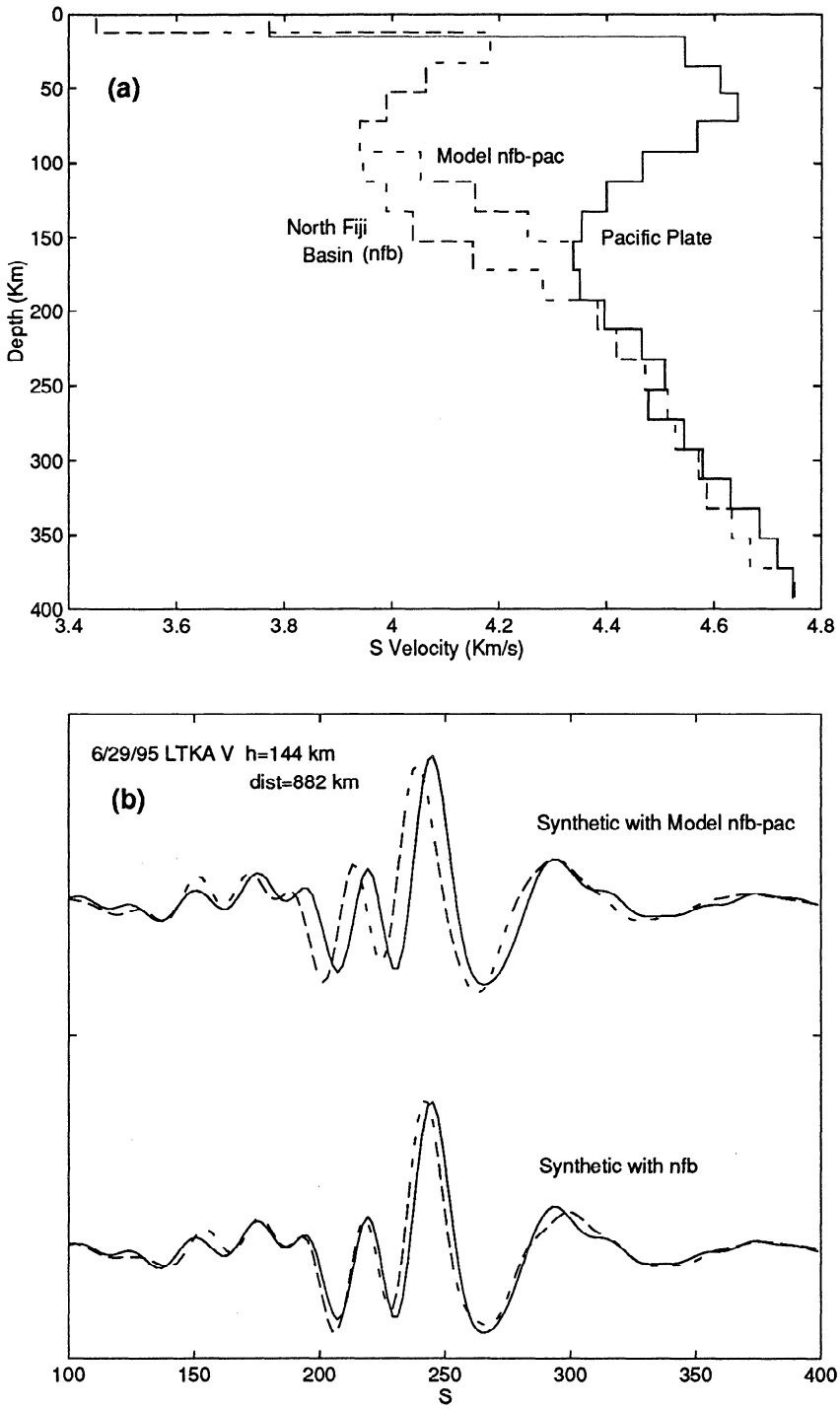

Figure 11. (a) A model nfb-pac, which limits differences between the North Fiji Basin and the Pacific Plate to depths <150 km, along with structures for the North Fiji Basin (nfb) and the Pacific Plate. This model is identical to the North Fiji Basin (nfb) structure above 90 km, to intermediate structures between the nfb and the Pacific structure between 90 and 150 km depth, and to the Pacific structure below 150 km. (b) Comparison of synthetic data (dashed line) with observed data (solid line) from an intermediate depth earthquake, with a propagation path traversing the North Fiji Basin. The synthetic data on the top is calculated with model nfb-pac, and the synthetic data on the bottom is calculated with model nfb. The *S* arrival and higher modes are poorly fit by the nfb-pac structure, illustrating the sensitivity of the waveforms from an intermediate depth earthquake to a low-velocity zone structure.

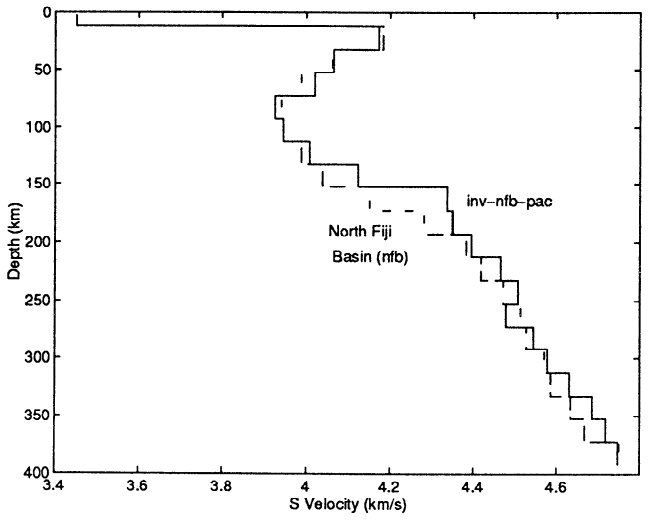

Figure 12. Shows squeezing test inversion results of inv-nfb-pac along with structure for North Fiji Basin (nfb). Model inv-nfb-pac was obtained in an inversion of North Fiji Basin data requiring structures below 150 km depth to be identical to the Pacific Plate. Model inv-nfb-pac shows higher residuals for intermediate depth earthquakes, indicating structures below 150 km are resolved.

structure (top) nfb-pac and (bottom) nfb. The synthetic data calculated with model (top) nfb-pac show significant misfit to the *S* wave and higher-mode arrivals, demonstrating the sensitivity of the synthetic data for low velocity zone structure.

To further test the depth extent of slow-velocity anomaly, we inverted the North Fiji Basin data using a model in which the structure below 150 km was fixed to the Pacific structure. This "squeezing" test was performed to see whether it is possible to find a model that fits the data with variations confined to shallower than 150 km. We began inversion with model nfb-pac but set the a priori model parameter above depth 150 km, as we did for inversion of final model nfb, so that we can avoid to the utmost bias of the effect of a priori information to the test result. The inversion result (model inv-nfb-pac) is shown in Figure 12. As we can see, the difference between model nfb and inv-nfb-pac is quite small above 130 km depth, which indicates that this part of the structure is well determined. To see if the Pacific structure below 150 km provides a good fit to the data, we calculated the misfit of waveforms from two intermediate depth earthquakes. The misfit calculated with model inv-nfb-pac is ~10% larger than that with model nfb, suggesting that the slow-velocity anomaly extending below 150 km depth is resolved for the North Fiji Basin.

Velocity anomalies below 170 km depth are much smaller, but a poorly resolved 2% velocity anomaly between the Lau Basin and the Pacific Plate persists to depths of 350 km. The inversion suggests that these differences are resolved at the level of one standard deviation. However, squeezing tests such as that described above for the North Fiji Basin suggest that the structure is not well resolved below 170 km for the Lau Basin, indicating that there is little resolution at these depths in the absence of a priori models. The limited depth resolution for the Lau Basin results from the short path lengths and thus shallower bottoming depths for paths traversing this region. Recent *P* wave tomographic results also using data from the Southwest Pacific Seismic Experiment find that the Lau Basin remains 2-3% slower than the Pacific lithosphere down to depths of 400 km [*Zhao et al.*, 1997], confirming that the slow velocities persist to greater depths. There has previously been considerable disagreement about the depth extent of slow-velocity anomalies at mid-ocean ridges, with some investigators favoring slow-velocity anomalies limited to depths of ~100 km [*Zhang and Tanimoto*, 1992, 1993; *Forsyth*, 1992], whereas others suggest that the slow velocities extend to depths of at least 300 km [*Su et al.*, 1992]. Our results show that for back arc spreading centers, anomalies >4% extend down to 170 km (Figure 10).

5. Conclusions

The basic conclusions of this study can be summarized as follows

1. Extremely large heterogeneity exists in the uppermost mantle of the southwest Pacific. The heterogeneity reaches a maximum of 18% at depths of 30-70 km between the active spreading Lau Basin and the old Pacific lithosphere.

2. Shear velocity just beneath the active Lau spreading center is as low as 3.8 km s^{-1}, which is considerably lower than previously found for mid-ocean ridges and may mark the lowest upper mantle velocity in the world. The very slow back arc velocities at depths of 30-90 km results from partial melting associated with seafloor spreading.

3. Heterogeneity >4% extends to depths of ~170 km.

4. The South Fiji Basin, an inactive back arc basin, also shows upper mantle velocities much slower than those found by previous studies of similarly aged lithosphere in the Pacific.

Acknowledgments. Equipment for the Tonga-Fiji seismograph deployment was obtained from the PASSCAL program of the Incorporated Research Institutions in Seismology (IRIS), a facilities program of the National Science Foundation. We thank P. Shore, P. Friberg, G. Hade, M. Bevis, K. Draunidalo, G. Prasad, and E. Roth for assistance in deploying and maintaining seismographs in the southwest Pacific. We also thank G. Randall for providing his efficient differential seismogram code, and D. Forsyth, S. van der Lee, and H. Paulssen for helpful reviews. This research was supported by the National Science Foundation under grants EAR 9219675, EAR9614502, and OCE9314446.

References

Aggarwal, Y. P., M. Barazangi, and B. Isacks, *P* and *S* travel times in the Tonga-Fiji region: A zone of low velocity in the uppermost mantle behind the Tonga island arc, *J. Geophys. Res.*, *77*, 6427-6434, 1972.

Anderson, D. L., Elastic wave propagation in layered anisotropic media, *J. Geophys. Res.*, *66*, 2953-2963, 1961.

Auzende, J. M., et al., Active spreading and hydrothermalism in North Fiji Basin (SW Pacific), Results of Japanese-French cruise Kaiyo 87, *Mar. Geophys. Res.*, *12*, 269-283, 1990.

Auzende, J. M., B. Pelletier, and Y. Lafoy, Twin active ridges in the North Fiji Basin (southwest pacific), *Geology*, *22*, 63-66, 1994.

Auzende, J. M., R. N. Hey, B. Pelletier, D. Rouland, Y. Lafoy, E. Gracia, and P. Hachon, Propagation rift west of Fiji archipelago (North Fiji Basin, SW Pacific), *J. Geophys. Res.*, *100*, 17, 823-17, 835, 1995.

Berteussen, K., Moho depths determinations based on spectral-ratio analysis of NORSAR long-period *P* waves, *Phys. Earth Planet. Inter.*, *15*, 13-27, 1977.

Bevis, M., et al., Geodetic observations of very rapid convergence and back-arc extension at the Tonga arc, *Nature*, *374*, 249-251, 1995.

Chapman, C. H., and J. A. Orcutt, The computation of body wave synthetic seismograms in laterally homogeneous media, *Rev. Geophys.*, *23*, 105-163, 1985.

Dubois J., G. Pascal, M. Barazangi, B. L. Isacks, and J. Oliver, Travel times of seismic waves between the New Hebrides and Fiji islands: A

zone of low velocity beneath the Fiji Plateau, *J. Geophys. Res.*, *78*, 3431-3436, 1973.

Dziewonski, A. M., and D. L. Anderson, Preliminary reference Earth model, *Phys. Earth Planet. Inter.*, *25*, 297-356, 1981.

Dziewonski, A. M., T. A. Chou, and J. H. Woodhouse, Determination of earthquake source parameters from waveform data for studies for global and regional seismicity, *J. Geophys. Res.*, *86*, 2825-2852, 1981.

Flanagan, M. P., Attenuation beneath back arc basins, Ph.D. thesis, Washington Univ., St. Louis, Mo., 1994.

Flanagan, M. P., and D. A. Wiens, Attenuation structure beneath the Lau back arc spreading center from teleseismic *S* phases, *Geophys. Res. Lett.*, *17*, 2117-2120, 1990.

Flanagan, M. P., and D. A. Wiens, Radial upper mantle attenuation structure of inactive back arc basins from differential shear wave measurements, *J. Geophys. Res.*, *99*, 15,469-15,485, 1994.

Forsyth, D. W., The early structural evolution and anisotropy of the oceanic upper mantle, *Geophys. J. R. Astron. Soc.*, *43*, 103-162, 1975

Forsyth, D. W., Seismological constraints on partial melting beneath the East Pacific Rise (abstract), *Eos Trans. AGU*, *73* (14), Spring Meet. Suppl., 290, 1992.

Fuchs, K., and G. Muller, Computation of synthetic seismograms with the reflectivity method and comparison with observation, *Geophys. J. R. Astron. Soc.*, *23*, 417-433, 1971.

Gaherty, J. B., T. H. Jordan, and L.S. Gee, Seismic structure of the upper mantle in a central Pacific corridor, *J. Geophys. Res.*, *101*, 22,291-22,309, 1996.

Hawkins, J. W., Evolution of the Lau Basin: Insights from ODP Leg 135, in *Active Margins and Marginal Basins of the Western Pacific*, *Geophys. Monogr. Ser.*, vol. 88, edited by B. Taylor and J. Natland, pp. 125-173, AGU, Washington, D. C., 1995.

Hawkins, J. W., and J.T. Melchior, Petrology of Mariana Trough and Lau Basin basalts, *J. Geophys. Res.*, *90*, 11,431- 11,468, 1985.

Kennett, B. L. N., *Seismic Wave Propagation in Stratified Media*, Cambridge Univ. Press, New York, 1983.

Kirkwood, S. C., and S. Crampin, Surface wave propagation in an ocean basin with an anisotropic upper mantle: Observations of polarization anomalies, *Geophys. J. R. Astron. Soc.*, *64*, 487-497, 1981.

Lerner-Lam, A. L., and T. H. Jordan, How thick are the continents?, *J. Geophys. Res.*, *92*, 14,007-14,026, 1987.

Luenberger, D. G., *Introduction to Linear and Nonlinear Programming*, Addison-Wesley, Reading, Mass., 1972.

Malahoff, A., S. R. Hammond, J.J. Naughton, D. L. Keeling, and R.N. Richmond, Geophysical evidence for post-Miocene rotation of the island of Viti Levu, Fiji, and its relationship to the tectonic development of the North Fiji Basin, *Earth Planet. Sci. Lett.*, *57*, 398-414, 1982.

McKenzie, D., and M. J. Bickle, The volume and composition of melt generated by extension of the lithosphere, *J. Petrol.*, *29*, 625-679, 1988.

Montagner, J. P., and T. Tanimoto, Global upper mantle tomography of seismic velocities and anisotropies, *J. Geophys. Res.*, *96*, 20, 337-20, 351, 1991.

Nishimura, C. E., and D. W. Forsyth, The anisotropic structure of the upper mantle in the Pacific, *Geophys. J.*, *96*, 203-229, 1989.

Nolet, G., Partitioned waveform inversion and two-dimensional structure under the network of autonomously recording seismographs, *J. Geophys. Res.*, *95*, 8499-8512, 1990.

Nolet, G., Seismic evidence for the occurrence of volatiles below 200 km depth in the Earth, in *Processes of Deep Earth and Planetary Volatiles*, edited by K. Farley, pp. 22-32, Am. Inst. Phys., New York, 1995.

Nolet, G., J. V. Trier, and R. Huisman, A formalism for nonlinear inversion of seismic surface waves, *Geophys. Res. Lett.*, *13*, 26-29, 1986.

Nolet, G., S. P. Grand, and B. L. N. Kennett, Seismic heterogeneity in the upper mantle, *J. Geophys. Res.*, *99*, 23,753- 23,766, 1994.

Parson, L. M., and I. C. Wright, The Lau-Havre-Taupo back-arc basin: A southward-propagating, multi-stage evolution from rifting to spreading, *Tectonophysics*, *263*, 1-22, 1996.

Randall, G. E., Efficient calculation of differential seismograms for lithospheric receiver functions, *Geophys. J. Int.*, *99*, 469-481, 1989.

Randall, G. E., Efficient calculation of complete differential seismograms for laterally homogeneous Earth models, *Geophys. J. Int.*, *118*, 245-254, 1994.

Sambridge, M., and G. Drijkoningen, Genetic algorithms in seismic waveform inversion, *Geophys. J. Int.*, *109*, 323-342, 1992.

Sclater, J. G., B. Parsons, and C. Jaupart, Oceans and continents: Similarities and differences in the mechanisms of heat loss, *J. Geophys. Res.*, *86*, 11,535-11,552, 1981.

Shearer, P. M., and J. A. Ocrutt, Compressional and shear wave anisotropy in the oceanic lithosphere: The Ngendei seismic refraction experiment, *Geophys. J. R. Astron. Soc.*, *87*, 967-1003, 1986.

Shen, Y., and D. W. Forsyth, Geochemical constraints on initial and final depths of melting beneath mid-ocean ridges. *J. Geophys. Res.*, *100*, 2211-2237, 1995.

Sinton, J. M., and P. Fryer, Mariana trough lavas from 18°N: Implications for the origin of back arc basin basalts, *J. Geophys. Res.*, *92*, 12,782-12,802, 1987.

Stein, C. A., and S. Stein, Comparison of plate and asthenospheric flow models for the thermal evolution of oceanic lithosphare, *Geophys. Res. Lett.*, *21*, 709-712, 1994.

Su,W. J., R. L. Woodward, and A. M. Dziewonski, Deep origin of mid-ocean-ridge seismic velocity anomalies, *Nature*, *360*, 149-152, 1992.

Su,W. J., R. L. Woodward, and A. M. Dziewonski, Degree-12 model of shear velocity heterogeneity in the mantle, *J. Geophys. Res.*, *99*, 6945-6980, 1994.

Sundaralingam, K., Upper mantle velocity of Fiji region from surface wave dispersion, *J. Phys. Earth.*, *34*, 407-426, 1986.

Tanimoto, T., and D. J. Stevenson, Seismic constraints on a model of partial melts under ridge axes, *J. Geophys. Res.*, *99*, 4549-4558, 1994.

Tarantola, A., *Inverse Problem Theory*, Elsevier, New York, 1987.

Taylor, B., K. Zellmer, F. Martinez, and A. Goodliffe, Sea-floor spreading in the Lau back-arc basin, *Earth Planet. Sci. Lett.*, *144*, 35-40, 1996.

Thompson, A. B., Water in the Earth's upper mantle, *Nature*, *358*, 295-302, 1992.

Trampert, J., and J. H. Woodhouse, Global phase velocity maps of Love and Rayleigh waves between 40 and 150 seconds, *Geophys. J. Int.*, *122*, 675-690, 1995.

Van Heijst, H. J., R. Snieder, and R. Nowack, Resolving a low-velocity zone with surface-wave data, *Geophys. J. Int.*, *118*, 333-343, 1994.

Weissel, J. K., and A. B. Watts, Tectonic complexities in the South Fiji marginal basin. *Earth Planet. Sci. Lett.*, *28*, 121-126, 1975.

Wiens, D. A., P. J. Shore, J. McGuire, E. Roth, M. G. Bevis, and K. Draunidalo, The southwest Pacific seismic experiment. *IRIS Newsl.*, *14*, 1-4, 1995.

Woodhouse, J. H., and A. M. Dziewonski, Mapping the upper mantle: Three-dimensional modeling of Earth structure by inversion of seismic waveforms, *J. Geophys. Res.*, *89*, 5953-5986, 1984.

Woodward, R. L., and G. Masters, Global upper mantle structure from long-period differential travel times, *J. Geophys. Res.*, *96*, 6351-6377, 1991.

Wyllie, P. J., Magmas and volatile components, *Am. Mineral.*, *64*, 469-500, 1979.

Zhang, Y. S., and T. Tanimoto, Ridges, hotspots and their interaction as observed in seismic velocity maps, *Nature*, *355*, 45-49, 1992.

Zhang, Y. S., and T. Tanimoto, High-resolution global upper mantle structure and plate tectonics, *J. Geophys. Res.*, *98*, 9793-9827, 1993.

Zhao, L., and D. V. Helmberger, Broadband modeling along a regional shield path, Harvard recording of the Saguenay earthquake, *Geophys. J. Int.*, *105*, 301-312, 1991.

Zhao, D., Y. Xu, D. A. Wiens, L. Dorman, J. Hildebrand, and S. Webb, Depth extent of the Lau back-arc spreading center and its relationship to deep subduction processes, *Science*, *278*, 254-257, 1997.

D. A. Wiens and Y. Xu, Department of Earth and Planetary Sciences, Washington University, 1 Brookings Drive, St. Louis, MO 63130 (email: yingbiao@izu.wustl.edu)

(Received May 9, 1997; revised September 2, 1997; accepted September 9, 1997.)